Characterizing hydrophobicity at the nanoscale: A molecular dynamics simulation study

ARTICLE *in* THE JOURNAL OF CHEMICAL PHYSICS · JUNE 2012

Impact Factor: 2.95 · DOI: 10.1063/1.4725185 · Source: PubMed

2 AUTHORS, INCLUDING:

Niharendu Choudhury
Bhabha Atomic Research Centre
57 PUBLICATIONS **1,060** CITATIONS

Characterizing hydrophobicity at the nanoscale: A molecular dynamics simulation study

Dibyendu Bandyopadhyay[1] and Niharendu Choudhury*

Theoretical Chemistry Section, Chemistry Group,

[1]*Heavy Water Division,*

Bhabha Atomic Research Centre, Mumbai 400 085, India

(Dated: February 6, 2012)

* Also at Homi Bhabha National Institute (HBNI), Mumbai. e-mail: nihcho@barc.gov.in & niharc2002@yahoo.com

Abstract

We use molecular dynamics (MD) simulations of water near nanoscopic surfaces to characterize hydrophobic solute-water interfaces. By using nanoscopic paraffin like plates as model solutes, MD simulations in isothermal-isobaric ensemble have been employed to identify characteristic features of such an interface. Enhanced water correlation, density fluctuation and position dependent compressibility apart from surface specific hydrogen bond distribution have been identified as characteristic features of such interfaces. Orientational distributions of the dipole moment vector and the molecular plane vector of the water molecule do not show much sensitivity to the nature of the surface, whereas that of OH bond vector shows enhanced structuring with increasing hydrophobicity. Tetrahedral order parameter that quantifies the degree of tetrahedrality in the water structure and an orientational order parameter, which quantifies the orientational preferences of the second solvation shell water around a central water molecule, have also been calculated as a function of distance from the plate surface. In the vicinity of the surface these two order parameters show considerable sensitivity to the surface hydrophobicity. The potential of mean force (PMF) between water and the surface as a function of the distance from the surface has also been analyzed in terms of direct and induced contributions, which shows unusual effect of plate hydrophobicity on the solvent induced PMF. In order to investigate hydrophobic nature of these plates, we have also investigated interplate dewetting when two such plates are immersed in water.

I. INTRODUCTION

Hydrophobic effect[1,2] is considered as one of the most sought after concept that provides rationale for apparently confusing phenomenon of assembly of hydrophobic groups in water and demixing of oil and water. Proximity of water to a hydrophobic surface dictates[3] its behavior and is thus fundamental to the so-called hydrophobic effect. Although its reason as well as definition is disputed, its importance in a variety of fields ranging from chemistry, biology, material science, chemical engineering is beyond doubts.

The concept of hydrophobicity[1,2,4,5] has long been used to explain many natural and synthetic phenomena and processes such as dissolution of inert gases in water, protein folding, colloidal stability, micelle formation, nanoparticle aggregation etc. At the macroscopic level, degree of hydrophobicity is generally assessed by measuring droplet contact angle.[6] In this conventional view, hydrophobicity is often characterized by an obtuse contact angle of water on a surface. In other words, water on a hydrophobic surface forms droplets in the form of beads, whereas it spreads on a hydrophilic surface. However, this view becomes obscure and sometimes ambiguous or untenable when translated into the molecular or even macromolecular domains. It remains a challenge[7,8] to define an unambiguous descriptor of hydrophobic solute-water interface at the nanoscopic lengthscales such as those involving proteins, micelles, nanoparticles, nanotubes etc., where defining a droplet is not possible. Sensitivity of hydrophobicity to solute-water dispersion interaction[9–13] and topography[14–16] poses additional challenge to define it.

It is well known that in smaller lengthscales[17–21] involving dissolution of inert gases in water, although molecular density distribution of water around the solute is quite high as compared to the bulk, a simple hard sphere model captures[17,20] hydration thermodynamics and the effects of temperature,[22,23] pressure[24] and added salt[25–27] quite successfully. At larger lengthscale, however water density distribution changes significantly from its molecular counterpart and generally for hard sphere model or purely repulsive model of the nanoscopic solutes, water recedes[28,29] from the solute surface, forming a thin vapor layer around the surface. When two such macroscopic hydrophobic surfaces approach each other, below a critical distance of approach cumulative effect of the fluctuations[30] of the individual surfaces leads to dewetting[29,31] of the intersolute region and this intersolute dewetting is sought[31] to be the origin of hydrophobic interaction that leads to self-assembly of hydropho-

bic groups as observed in the core of a protein or a micelle. At the nanoscopic and larger lengthscales, theory[29,32] and many simulations[10–12,33–42] have captured this picture. It was also demonstrated[43] that hydration free energy of a hydrophobic solute scales with volume at small lengthscales and with surface area at larger length scales and the crossover between the two occurs at the nanometer length scale.

Apart from thermodynamic conditions, behavior of hydrophobic hydration and interfacial water dynamics are also dependent on solute-water dispersion interaction. It has been thoroughly demonstrated[10–12,35,36,44] how dispersion interaction changes hydration behavior as well as thermodynamics. Several recent studies[15,16,41,42] have demonstrated that surface topography has so significant influence on the hydration behavior that only by controlling the topography of the solute surface one can create dry, wet or oscillatory (with time) wet-dry state of the intersolute region. Therefore understanding hydrophobicity has been a challenge of multidimensional nature in the space of parameters such as thermodynamic conditions, lengthscale, solute-water dispersion interaction, solute topography etc.[45] Recent studies[46] have analyzed contributions of these different parameters on the manifestation of hydrophobicity by separating geometry or topography from chemistry that determines hydrophobic/hydrophilic nature of an engineered protein surface. It has also been shown[47] that surface hydrophobicity can be enhanced by suitably coupling polarity of the surface with its topography. As far as understanding the molecular mechanism of protein folding is concerned, two limiting views have so far emerged.[46,48] In one case, the traditional view that water density is gradually reduced in the intersolute region in a manner concerted with their spatial approach toward each other. Thus water evacuation here is a gradual process. In the alternative scenario, due to thermodynamic instability, expulsion of all the water from the intervening space between large hydrophobic domains leads to cavitation and then follows the so-called hydrophobic collapse.[29,31,33] In the later case, the process of self-assembly is a two steps process. Recent discussion and analyses as summarized from available protein folding studies however suggest[48] that the two-step cavitation pathway is not the actual pathway in most of the cases, rather water has involvement in almost all the stages of the folding landscape. On the other hand, cavitation may play an important role in experimentally observed[49–51] long-ranged attraction between two hydrophobic surfaces when they are put into water. However, the range of attraction as observed in these experiments is much more than what most of the theoretical[29] and computational[12] studies have predicted

on the basis of even idealized hard body model.

Recent studies of Berne and coworkers with BphC[44] and melittin tetramer[14] in water have clearly demonstrated how sensitive is this dewetting or cavitation to the nature of protein surface in terms of geometry, chemistry and presence of specific residue. In case of BphC, no cavitation was observed in the interdomain region where water can sterically access the region. However by turning off the electrostatic interactions between the protein and the water, dewetting did results. On the other hand, for melittin tetramer cavitation was observed even with usual electrostatic interactions, but it disappeared by altering the geometry through specific mutations. Actually this mutation altered the surface topography by removing protruding hydrophobic side chains. All these studies have pointed out the subtleness of defining hydrophobicity at the nanoscale.

One convenient way of predicting hydrophobicity from molecular dynamics simulation is through calculation of (molecular level) local density of water as calculated by averaging over all the relevant configurations. A fundamental question arises in this case that whether such an averaged out picture of the local density can provide a true and quantitative measure of hydrophobicity of a realistic surface. Given the fact that microscopic fluctuations are inherent[30] to such a hydrophobic interface, characterization of hydrophobic solute-water interface in terms of local density, which can not capture these fluctuations, is not enough. Very recently Garde and coworkers[8,45] have tried to address this issue and have come up with some descriptors to characterize[7,8] the solute-water interface. It is shown[8] that local density description is ambiguous in many cases, but free energy of hydration of small solutes near the surface and position dependent as well as average solvation shell compressibility and solvent induced solute-water PMF can be used to characterize such a solute-water interface.

In the present investigation, we extend this study and show that various other descriptors such as hydrogen bond distribution, orientational orders of the water molecules in the second shell of a central molecule, distributions of various orientational vectors of the water molecule near the plate, tetrahedrality parameter can also be used to characterize hydrophobic solute-water interfaces. We examine suitability of a number of such descriptors for the characterization of nanoscale solute/surface-water interfaces. We have created various plates with varying degrees of hydrophobicity by arranging five paraffin molecules side by side. Plates with varying hydrophobicity are created just by varying the affinity of these molecule for water through the modification of the dispersion interaction between the water

oxygen and surface carbon atoms. Along with the above mentioned descriptors, we have also calculated position dependent compressibility, solvent density fluctuation, water-water correlation, induced potential of mean force between a water molecule and the surface, apart from calculating one-particle density distribution of the oxygen atom and hydrogen atom of the water molecules. We have examined how these descriptors respond to the change in the degree of hydrophobicity as achieved by tuning the van der Waals interaction between water and the carbon atoms of the solute plate.

Generally, a nanoscopic or larger hydrophobic solute dewets its immediate vicinity at the Angstrom lengthscale. But when two such hydrophobic solutes are immersed in water, at a certain critical intersolute distance all the water molecules get expelled from the intersolute region and two solutes collapse, leading to dewetting induced collapse. This is one of the most soughtafter[28,29,31] plausible pathways for protein folding. In the present investigation, we have therefore investigated whether interplate dewetting exists between any such pair of plates. We found dewetting in almost all the cases, but critical distance for dewetting depends on the degree of hydrophobicity. In what follows, we describe simulation model and method along with a brief description for various analysis in Sec II. Results and discussion have been presented in Sec. III and a few concluding remarks in Sec. IV.

II. MODELS & METHODS

We consider a planar model of solute consisting of paraffin-like molecules by placing a number of *n*-$C_{18}H_{38}$ molecules arranged in parallel in such a way that all the carbon atoms are lying on the same plane. For the alkane molecule, the united atom OPLS (OPLSUA) force field[52] has been used. In this description, both CH_3 and CH_2 groups are modeled as uncharged spherical sites with Lennard-Jones (LJ) interactions, with no explicit consideration of the hydrogen atoms. The LJ parameters for the CH_3 group according to the OPLSUA force-field are $\sigma_{CH_3-CH_3} = 3.905$ Å and $\epsilon_{CH_3-CH_3} = 0.7322$ kJ/mol and those for CH_2 group are $\sigma_{CH_2-CH_2} = 3.905$ Å and $\epsilon_{CH_2-CH_2} = 0.4937$ kJ/mol. In order to prepare various plates of different degree of hydrophobicity, we have varied ϵ values through a parameter λ such

that site-site interaction between CH_3 or CH_2 group and water oxygen follows

$$u(r) = 4\epsilon \left[\left(\frac{\sigma}{r}\right)^{12} - \lambda \left(\frac{\sigma}{r}\right)^{6} \right], \tag{1}$$

where $\lambda = 1$ corresponds to the the original OPLSUA parameters. We have used a paraffin-like plate of roughly the dimension (center to center distance) of 11 Å $\times$ 12 Å. Water has been modeled by the standard SPC/E[53] potential in which there are one LJ center and three charge centers coinciding with the three atoms of the water molecule. For solute-water interaction, the cross parameters for the LJ potential were obtained from the Lorentz-Berthelot mixing rule. One solute plate was placed in the middle of a water box with the plane of the plate parallel to the xy-plane of the box. All the water molecules from the immediate vicinity of the plate were removed followed by a steepest decent minimization.

The simulations were performed in isothermal isobaric (NPT) ensemble with molecular dynamics extended system approach of Nose and Anderson.[54] Periodic boundary conditions were applied in all three directions and Ewald method was applied to compute electrostatic interactions among all the water molecules. The bonds and the angle of the water molecule were constrained by using RATLE algorithm.[54] The solute plates were kept rigid and fixed during the simulation run. Equations of motion were integrated using velocity Verlet algorithm with 2 fs time step. All the simulations were carried out at a target temperature of 298 K and a target pressure of 1 atm. Each of the simulation runs was 2 ns or longer.

To study the spatial structure such as one-particle density distribution, and hydrogen-bond distribution around the solute plate, we have considered only those water molecules residing within a rectangular box of the dimensions of the solute plates in x and y-directions and of the size of the simulation box in z-direction. For the analysis of fluctuation as well as compressibility as calculated from the pressure dependence of the local density, we considered a rectangular slab of water molecules at different values of z (corresponding to different perpendicular distances from the plate) with the size of the slab considered to be the size of the solute plates in x- and y-direction and a width of 1 Å in z-direction. For calculation of compressibility, we have first calculated density of water at different slabs using simulation trajectories at different pressures P =1, 150, 300, 500, 1000, 2000 bars. Finally position dependent compressibility, $\chi_T(z)$ is calculated[7] from the derivative of density, $\rho(z)$ with respect to pressure, P, viz.

$$\chi_T(z) = \frac{1}{\rho(z)} \left(\frac{\partial \rho(z)}{\partial P} \right)_{\Delta,T} \tag{2}$$

where z is the location of the center of the slab and Δ is the slab thickness. We have calculated the derivative from the fitting[7,55] of the density versus pressure data to a second order polynomial. For the calculation of density fluctuation, we used calculated normalized fluctuation[30] in the number of water molecules within a specific volume, viz.

$$\kappa_N = \frac{[\langle N^2 \rangle - \langle N \rangle^2]}{\langle N \rangle} \tag{3}$$

where $\langle \cdots \rangle$ denotes ensemble average.

III. RESULTS & DISCUSSIONS

A. Hydration characteristics of single plate

As stated earlier, in this investigation, we have considered various model paraffin-like plates differing from each other only in the Lennard-Jones interaction with the oxygen of water according to Eq. (1) with different λ values. Decreasing values of λ correspond to increasing degree of hydrophobicity of the plate. In Fig. 1, plots of normalized single-particle distributions of water oxygens, $g_{SO}(z)$ $(= \rho(z)/\rho_0)$ as a function of the distance, z from the plate for various values of λ are shown. Here the values of λ considered are 0.0, 0.25, 0.50, 0.75 and 1.0, in which $\lambda = 1.0$ corresponds to the ϵ parameter of the OPLSUA force-field. It is clearly seen that for $\lambda = 0.0$, water recedes from the interface and the density profile looks like that of a liquid-vapor interface. This is in agreement with many previous theoretical and computational investigations,[29] in which it is demonstrated that a thin vapor layer exists in the vicinity of the hydrophobic solute in water. So for a purely repulsive solute we have also found that there is a depletion zone surrounding the solute plate and the width of the depletion layer, as obtained from the distance of the mid-density plane from the plate, is around 3 Å in the present case. As the value of λ is increased from 0 to 0.25, which corresponds to considering a very small attraction in the interaction between solute atom and the oxygen of water, the density profile is pulled closer to the plate surface slightly, although the overall nature of the density profile still resembles that of a liquid-vapor interface. In this case, the width of the depletion region is reduced and it is around 2.5 Å. For $\lambda = 0.5$, increased attraction changes the nature of the plot and now

the sigmoidal nature of the density plot as observed in case of $\lambda = 0.0$ or 0.25, which are reminiscent of liquid-vapor interface, has been changed to a liquid like density profile with peaks and troughs defining solvation layers. For $\lambda = 0.75$ and 1.0, there are pronounced peaks and troughs in the density profile and the first peak adjacent to the wall is as enhanced as about twice that of the bulk density and it looks like that the paraffin surfaces with this parameter sets are hydrophilic. Thus by changing the parameter λ from 0 to 1 we are able to create various paraffin-like plates that behave like hydrophobic to hydrophilic as far as local density distribution of water is concerned.

As evident from the local density distribution of water around the plate, water experiences different forces from different plates (with different λ values). One can thus represent the density distribution plots in terms of potential of mean force (PMF) between the plate and a water molecule $W_{SO}(z)$ by calculating it using the relation

$$\begin{aligned} W_{SO}(z) &= -k_B T \ln g_{SO}(z) \\ &= U_{SO}(z) + \omega_{ind}(z), \end{aligned} \tag{4}$$

where k_B is the Boltzmann constant, T is temperature, $U_{SO}(z)$ is the direct interaction energy between water and the plate and $\omega_{ind}(z)$ is the solvent induced contribution to the overall PMF. The solvent induced contribution $\omega_{ind}(z)$ is a measure of the indirect effect of all the other water molecules. As it is displayed in Fig. 2(a), the PMFs for $\lambda = 0.0$ is repulsive throughout the whole separation range, whereas for $\lambda = 0.5$ or 1.0 there are regions of plate-water separations (z values) for which PMF is negative, manifesting attraction. The corresponding solvent induced PMFs $\omega_{ind}(z)$ show interesting behavior as a function of λ. For $\lambda = 0.0$ i.e. when the paraffin wall is purely repulsive, the solvent induced contribution $\omega_{ind}(z)$ shows a barrier at around $z = 4$ Å , below which the value is negative. As the value of λ is increased to 0.25 and then to 0.5, the barrier height at $z = 4$ Å decreases, but another barrier is formed at around 6 Å. As the value of λ is increased further to 0.75 and then to 1.0, a broad shoulder region is formed with a steep barrier height starting from 6 Å downwards till 4 Å. Thus addition of attractive interaction in the interaction potential between solute site and water surprisingly makes the solvent induced contribution positive. Thus water molecule in the hydration shell prevents the test molecule from entering into it from the bulk. This has already been observed[56] in case of hydration of methane and fullerenes of different sizes. The barrier in induced PMF on approaching the plate can be understood by assuming

$\omega_{ind}(z)$ as correction to the huge increase in density in the vicinity of the solute plate due to attractive interaction according to the Boltzmann response, $g_{SO}|_{\lambda=0} \exp[-U_{SO}^{att}/K_BT]$. Therefore as the value of λ increases, attractive interaction increases and therefore density at the contact should increase to a very high value according to the above equation, but increased positive $\omega_{ind}(z)$ value at high λ corrects the excess density probably by forming a repulsive core packing due to solvation shell waters and/or hydrogen bonding constraints.[56]

In oder to investigate the average orientational preference of water near the surface, we have considered a rectangular slab of water molecules of the dimensions of the solute in x- and y-directions and of width 1 Å in the z-direction and calculated orientational distributions of the three orientational vectors of the water molecule namely, dipole moment vector (μ), OH vector and a vector perpendicular to the molecular plane of a water molecule. The angles made by the vectors μ, OH and a vector perpendicular to the paraffin plate (i.e. plane vector) with outward (solute) plate normal vector are represented by θ, ψ and ϕ respectively. These orientational distributions are shown in Fig.3. The distribution for the dipole moment vector $\mathrm{P}_{\mu}(\cos\ \theta)$ vs $\cos\theta$ as shown in Fig. 3(a) does not show much change with change in λ or attractive interaction of the solute. In case of OH bond vector, we observe (see Fig. 3(b)) a noticeable change in the intensity of the distribution $\mathrm{P}_{OH}(\cos\ \psi)$, but positions of the peaks of the distribution remain almost unchanged with λ. There is an increase in peak height at around $\cos\theta = -0.25$ indicating a preferred orientation of OH bond pointing the paraffin plate at large λ value. The distribution of the molecular plane vector $\mathrm{P}_{\perp}(\cos\ \phi)$ of the water molecule also does not change much with the change in λ, except that intensity changes at two values of θ viz., 0° and 180°. Thus orientational distributions of water are not so sensitive to the degree of hydrophobicity of the plate.

Histograms of hydrogen bond (H-bond) distribution of the water molecule having n H-bonds are displayed in Fig 4(a)-(f). The fraction of molecules having n H-bonds f_n^{HB} are shown as a function of number of H-bonds n_{HB}. These are calculated for water molecules residing in a 1 Å wide slab parallel to the solute plate at a distance 3.5 Å from the plate and the slab dimension in x and y-directions are the same as the dimensions of the solute plate. For $\lambda = 0.0$ plate (Fig. 4(a)), almost 50 % of the water molecules have 2 H-bonds and 35 % have 3 H-bonds. As the value of λ increases from zero to 0.25 (Fig. 4(b)), the fraction of molecules having 2 H-bonds decreases where as those having 3 H-bonds increases and at $\lambda = 0.5$ (see Fig. 4(c)), population having 3 H-bonds f_3^{HB} crosses over to that (f_2^{HB}) having 2

H-bonds. Along with this, fraction having 4 H-bonds also increases marginally. As we go on increasing λ further, fraction of molecules having 3 H-bonds increases whereas those having 2 H-bonds decreases and f_3^{HB}reaches almost 50 % at $\lambda = 1$. If this result is compared with the same for bulk (see Fig. 4(f)), we find that in the bulk, almost 50 % of the molecules have 4 H-bonds and 35 % have 3 H-bonds. Thus even for the plate having maximum degree of hydrophilicity ($\lambda = 1$) considered here, fraction of molecules having 4 H-bonds are quite less (20 %) as compared to the bulk. Thus the presence of the solute plate in one side of the water slab introduces geometric frustration and reduces the number of molecules having 4 H-bonds. We have also calculated average number of H-bonds ($< n_{HB} >$) as a function of perpendicular distance from the plate. It is observed (see Fig. 5) that far away from the plate where water behaves like bulk water, average no of H-bonds are about 3.5 and from around 6 Å and below number of H-bonds decreases and reaches the value of 2-2.5 at around $z = 2 - 2.5$ Å from the plate depending on the λ values. In case of $\lambda = 0.0$, the depletion zone ends around 8 Å. On the other hand, minimum distance at which n_{HB} goes to zero is more for $\lambda = 0$ plate.

Another quantity which may be a yard stick to measure hydrophobicity is the isothermal compressibility[8] of water in the vicinity of the solute surface. In order to calculate this quantity, we have simulated a systems with a particular value of λ at different pressures as mentioned in Sec II and from the simulation trajectory we have calculated density of water in a slab of width 1 Å placed at various positions parallel to the plate. From the pressure dependence of the density (cf. Eq.(2)), $\chi(z)$ is calculated. As shown in Fig.6, the compressibility value of the system with $\lambda = 1.0$ and 0.5 are very low everywhere, whereas that for plate with $\lambda = 0.0$ is very high near the surface. The increase in compressibility of water near a hydrophobic surface has already been observed for self-assembled monolayer-water, protein-water interfaces.[7,8] Thus compressibility is a good descriptor of hydrophobic solute-water interface. However calculation of compressibility through this route is computationally demanding as we require to simulate the system at various pressures. An alternative to this compressibility could be the water density fluctuation as calculated by the variance in the number of water molecules normalized by mean in a specific slab volume at a particular distance from the plate surface (cf. Eq. (3)). In the macroscopic limit, in an open system this ratio κ_N approaches $\rho\, k_B\, T\, \chi_T(z)$. The κ_N values as a function of slab distances from the solute plate is shown in Fig.7. It is seen that fluctuations for $\lambda = 1.0$ is just like bulk

fluctuation. For $\lambda = 0.75$, only at $z = 3.5$ fluctuation is more, while for other values of z, it is the same as the $\lambda = 1.0$ case. Fluctuation is maximum in case of plates with $\lambda = 0.0$ i.e for the most hydrophobic plate. This quantity at low distances (upto 3.5) shows considerable fluctuation even for $\lambda = 0.5$ case, which is in contrast to the χ_T variation. This is because the average number of water molecules $< N >$ at low z is very small and since it appear in the denominator of Eq. (3), the normalized fluctuation becomes quite high. However, at $z = 4.0$ Å, the variation of κ_N is of the same nature of χ_T. The calculation of κ_N is computationally not expensive and therefore easier to use. The value of κ_N for the repulsive plates with λ values 0.0 and 0.25 exceed the ideal gas limit of 1 and this super-Poissonian statistics may be due to contributions from weak clustering to the density fluctuation.[30]

A structural measure, sensitive to the degree of hydrophobicity of the solute (value of λ here) is the water-water correlation as obtained from the radial distribution function of the oxygen atoms of water, $g_{OO}(r)$ in a 1 Å wide slab parallel to the plate. It is clearly seen from Fig. 8(a) that the two-particle correlation, $g_{OO}(r)$ shows nice variation with the surface hydrophobicity (i.e with λ). When λ is large i.e degree of hydrophobicity of the surface is less, peak in the correlation is smaller as compared to the same when λ is small i.e when degree of hydrophobicity of the surface is more. It is important to note that even the peak height for the least hydrophobic plate considered here ($\lambda = 1.0$) is more than that of the bulk and thus the plate with $\lambda = 1.0$ also has considerable signature for hydrophobicity. Similar correlation has also been observed for intermolecular oxygen-hydrogen correlation as calculated through $g_{OH}(r)$ within the slab. Plots of $g_{OH}(r)$ for different λ values are shown in Fig 8(b). For comparison, the same is shown for bulk water. There is enhanced correlation in the intermolecular oxygen-hydrogen correlation among the water molecules in the slab for water near plate with higher degree of hydrophobicity. Thus the water correlation within a narrow slab parallel to the solute plate also can be used to characterize hydrophobic solute-water interface. However, as the change in the peak height is gradual with the increase in λ it is difficult to identify the crossover between hydrophobic and hydrophilic surfaces.

Water is a network forming liquid with tetrahedral configuration of the water molecules. In order to quantify the degree of tetrahedrality various order parameters have been proposed and used[57–59] for bulk water. In the vicinity of a hydrophobic plate, it is expected that the tetrahedral structure of water will be disrupted and therefore an order parameter measuring tetrahedrality of water as a function of distance from the solute plate will be a good predictor

for hydrophobicity. Here the order parameter corresponding to the central water molecule i is defined[57,58] as

$$q_i \equiv 1 - \frac{3}{8}\sum_{j=1}^{3}\sum_{k=j+1}^{4}\left[\cos\,\theta_{jik} + \frac{1}{3}\right]^2 \tag{5}$$

where θ_{jik} is the angle formed between neighbors j and k and the central molecule i. The average value for a given set of molecules

$$q_4 = \frac{1}{N_s}\sum_{i=1}^{N_s} q_i \tag{6}$$

quantifies the tetrahedral order of the system. When we calculate this parameter in the vicinity of the plate, we extend the above definition and consider that the four nearest neighbors of the central molecules may be water or a solute carbon atom. In the above expression N_s is the number of central molecules considered in the given set. This definition is a slightly modified version of the parameter introduced in Ref.[57]. In an ideal gas $q_4 = 0$ and for a perfect tetrahedral network $q_4 = 1$. Thus q_4 measures the degree of tetrahedrality in the distribution of four nearest neighbors around a central water oxygen atom. In the present case, we have calculated q_4 for (central) water molecules residing in a slab of width 1 Å parallel to the plate and of the dimension of the plate in the other two directions. In Fig. 9(a) the plots of q_4 as a function of the distance of the center of the slab from the plate, z for different values of λ are presented. In all the cases q_4 values near the surface are small and as the distance of the plate increases q_4 value increases and eventually reaches steady bulk value. The distance from the plate at which q_4 reaches the bulk value depends on the degree of hydrophobicity of the plate (i.e. on the value of λ). For the most hydrophobic plate ($\lambda = 0$), effect of the plate on the tetrahedrality extends upto 8.5 Å, whereas for the least hydrophobic plate (plate with $\lambda = 1$), it extends only upto 5 Å. Near the plate deviation from tetrahedrality is more as compared to the same away from the plate. At around 2.5 Å, the q_4 value is as low as -0.2 for the most hydrophobic plate (i.e. $\lambda = 0.0$) and it increases to 0.27 for the least hydrophobic plate (i.e. $\lambda = 1.0$) considered here. In the inset of Fig.9(a) we have shown the q_4 values for the slab of water adjacent to the solute plate as a function of degree of hydrophilicity λ and it shows that with the increase of λ, q_4 increases steadily.

In case of a hexagonal crystal, the second shell forms an *hcp* structure and therefore an orientational order parameter for the second shell molecule around the central molecule i,

Q_{6i}, which quantifies the extent to which the central molecule i and twelve of its second shell neighbors forms a *hcp*, *fcc* or *bcc* structure is defined. In order to compute Q_{6i}, we first define[59] twelve bonds connecting the central molecules with its twelve next neighbors in the second shell and compute for each bond its azimuthal and polar angles (θ, ϕ). Next we calculate $\bar{Y}_{lm}(\theta, \phi)$, the average of the spherical harmonics over 12 bonds of the central molecule i. From this $\bar{Y}_{lm}(\theta, \phi)$, finally the function

$$Q_{li} \equiv \left[\frac{4\pi}{2l+1} \sum_{m=-l}^{m=l} |\bar{Y}_{lm}|^2 \right]^{1/2} \tag{7}$$

is calculated. For $l = 6$, the average value for a set of N_s central molecules

$$Q_6 = \frac{1}{N_s} \sum_{i=1}^{N_s} Q_{6i} \tag{8}$$

quantifies the orientational order of the set of molecules in the second shell around the central molecule. This parameter is large for most crystals and for perfect *hcp*, *bcc* and *fcc* structures Q_6 values are 0.485, 511 and 0.574 respectively. Fig.9(b) shows the Q_6 parameters as calculated by taking all the central molecules residing in the slab of width 1 Å parallel to the plate as a function of the position of the slab with respect to the plate, z. As in the case of q_4, the value of Q_6 also is very low in the vicinity of the surface and increases with the increase of the distance from the plate surface, and saturates to the bulk value at sufficiently large distances. The influence of the plate on this orientational parameter is also maximum for the most hydrophobic plate ($\lambda = 0.0$) and the least for the least hydrophobic plate ($\lambda = 1.0$). At around $z = 2.5$ Å, value Q_6 for $\lambda = 0.0$ is the minimum and increases gradually as the value of λ increases i.e. degree of hydrophobicity decreases. However the change of the Q_6 with λ in the vicinity of the plate is not as much as change in q_4.

B. Interplate dewetting

In order to investigate dewetting in the interplate region, we have considered two plates immersed in water. We considered all five plates with λ values 0.0, 0.25, 0.5, 0.75 and 1.0. In Fig. 10(a), the one-particle density of water in and around the two-plates system is shown for the most hydrophilic i.e. $\lambda = 1.0$ plate-water system at an interplate distance of 7.5 Å. A very sharp peak in the middle of the two plates as well as at the outside

surfaces of the plate shows hydrophilic nature of the plates and there is no dewetting in the middle. In this interparticle distance geometrically only one layer of water molecules can be accommodated. The same for $\lambda = 0.75$ plate-water system is shown in Fig. 10(b)). When interplate distance, r_0 is increased from 7.5 Å to 10 Å, there is no density peak of water in the middle i.e. there is no water in the middle of the two plates (see black plot of Fig. 10(b)). It is important to mention that although there is no density peak in the middle, the density peaks adjacent to outside surfaces of the plates are high and sharp indicating wet interfaces. This indicates that even when each of the individual plates is wet, combined fluctuations of the two plate-water interfaces in the intersolute region induce dewetting. However when the distance between the two plates is increased to 12 Å , water enters into the middle as evidenced by the two distinct peaks in the middle (see red lines in the same plot). Thus for $\lambda = 0.75$ plate, the critical distance for dewetting is around 10 Å.

In Fig.11, we have shown density profiles of water for $\lambda = 0.5$ and $\lambda = 0.0$ plates. In case of $\lambda = 0.5$ plates (Fig. 11(a)), the space between the two plates is dewetted upto interplate distance r_0 of 12 Å. When the interplate distance is changed to 14 Å, there are density peaks in the middle (see the red graph in Fig. 11(a)). Although not so sharply defined, there are almost three peaks in the middle, indicating that the intersolute space is enough to accommodate three water layers. However a slight decrease of r_0 value dewets the interplate region and there is no existence of two- or one-layer water between the plates. For $\lambda = 0.0$ plates however, we always found dewetted interplate region upto interplate distance of $r_0 = 16$ Å (see Fig. 11(b)). It is interesting to observe that in this case, density peaks adjacent to two outside surfaces are also flat and sigmoidal in shape, which is reminiscent to the liquid-vapor interface. Thus, we found that except $\lambda = 1.0$ plate, which is completely hydrophilic, all other plates show dewetting at some critical distance.

IV. CONCLUDING REMARKS

In order to characterize hydrophobic solute-water interface at the nanoscale we have calculated various structural and thermodynamic quantities relating to water structure and thermodynamics in the vicinity of hydrophobic surfaces. At the nanoscale it is difficult to use the macroscopic contact angle criterion to characterize such an hydrophobic interface. Here we varied the hydrophobicity of the plate by changing the energy parameter of the

solute-water non-bonded LJ interaction through a parameter λ (see Eq. (1)). It is already demonstrated[11] that the non-bonded energy parameter is a good tunning parameter, variation of which can create wet, dry or intermittent wet-dry state in the intervening region between two nanoscopic plates. In the present study, we have calculated various structural quantities such as single-particle density of water and average number of H-bonds as a function of distance from the surface, three different orientational distributions of water, H-bond histogram, isothermal compressibility as calculated through the pressure derivative of the water density, water number fluctuations, in-plane radial distribution of water, tetrahedral and Q_6 orientational order parameter and a thermodynamic quantity namely, the potential of mean force of a water molecule with the hydrophobic surface. Out of all these quantities, orientational structure of water does not depend much on the surface hydrophobicity. All other quantities show considerable variation with respect to degree of hydrophobicity of the plate. The solvent induced contribution to the PMF of a water molecule with the plate shows unusual behavior in that addition of attraction to the plate-water interaction although decreases the barrier height, widens the width of the barrier. This is observed till $\lambda = 0.75$ and when the attractive interaction is further increased the barrier height as well as width increases beyond that of the $\lambda = 0.0$ case. In case of tetrahedral order parameter and Q_6 orientational parameter also a clear distinction appears for water near the hydrophobic and hydrophilic plates. The dewetting between two plates has also been investigated and it is found that the critical distance for dewetting varies with the degree of hydrophobicity of the plate as described by the parameter λ.

However, variation of these descriptors with λ is gradual and no clear cut threshold values of these descriptors for defining hydrophobic or hydrophilic interfacial behavior can be assigned. All these structural and thermodynamic parameters can respond to the degree of hydrophobicity of the plate, but no distinct demarcation exists between the hydrophobic and hydrophilic solute-water interfaces. Since it is well known that manifestation of hydrophobicity is lengthscale dependent, it is also important to know how these quantities vary with the lengthscale of the hydrophobic solutes and investigation in this direction is in progress.

Acknowledgments

The author is thankful to Dr. S. K. Ghosh and Dr. T. Mukherjee for their kind interest

and encouragement. It is a pleasure to thank Computer Division, B.A.R.C., Mumbai, for providing Anupam supercomputating facilities and support.

[1] C. Tanford, *The Hydrophobic Effect: Formation of Micelles and Biological Membranes*, John Weiley: New York, 1973.

[2] W. Kauzmann, Adv. Protein Chem. **14**, 1 (1959).

[3] S. Granick, S. C. Bae, Science, **322**, 1477 (2008).

[4] L. R. Pratt, A. Pohorille, Chem. Rev. **102** , 2671 (2002); H. S. Ashbaugh, L. R. Pratt, Rev. Mod. Phys. **78**, 159 (2006).

[5] B. Ben-Naim, *Hydrophobic Interactions*, Plenum: New York, 1980).

[6] T. Werder, J. H. Walther, R. L. Jaffe, T. Halicioglu, P. Koumoutsakos, J. Phys. Chem. B **107**, 1345 (2003).

[7] H. Acharya, S. Vembanur, S. N. Jamadagni, S. Garde, Faraday Discuss. **146**, 353 (2010).

[8] R. Godawat, S. N. Jamadagni, S. Garde, Proc. Natl. Acad. Sci. U.S.A. **106**, 15119 (2009).

[9] H. S. Ashbaugh, M. E. Paulaitis, J. Am. Chem. Soc. **123**, 10721 (2001).

[10] N. Choudhury, B. M. Pettitt, J. Am. Chem. Soc. **127**, 3556 (2005).

[11] N. Choudhury, B. M. Pettitt, J. Am. Chem. Soc. **129**, 4847 (2007).

[12] X. Huang, C. J. Margulis, B. J. Berne, Proc. Natl. Acad. Sci. U.S.A. **100**, 11953 (2003).

[13] N. Choudhury, B. M. Pettitt, *in Modelling Molecular Structure and Reactivity in Biological Systems* pp. 49, RSC Publishing, **31**, 49-57 (2005).

[14] P. Liu, X. Huang, R. Zhou, B. J. Berne, Nature **437**, 159 (2005).

[15] N. Choudhury, J. Phys. Chem. B **112**, 6296 (2008).

[16] N. Choudhury, J. Chem. Phys. **131**, 014507 (2009).

[17] L. R. Pratt, D. C. Chandler, J. Chem. Phys. **67**, 3683 (1977).

[18] C. Pangali, M. Rao, B. J. Berne, J. Chem. Phys. **71**, 2975 (1979).

[19] D. E. Smith, A. D. J. Haymet, J. Chem. Phys. **98**, 6445 (1993).

[20] G. Hummer, S. Garde, A. E. Garcia, A. Pohorille, L. R. Pratt, Proc. Natl. Acad. Sci. U.S.A. **93**, 8951 (1996).

[21] N. T. Southall, K. A. Dill, Biophys. Chem. **101**, 295 (2002).

[22] B. Guillot, Y. A. Guissani, J. Chem. Phys. **99**, 8075 (1993).

[23] S. Garde, A. E. Garcia, L. R. Pratt, G. Hummer, Biophys. Chem. **78**, 21 (1999).

[24] G. Hummer, S. Garde, A. E. Garcia, M. E. Paulaitis, L. R. Pratt, Proc. Natl. Acad. Sci. U.S.A.

95, 1552 (1998).

[25] P. E. Smith, J. Phys. Chem. B **103**, 525 (1999).

[26] A. Kalra, N. Tugcu, S. M. Cramer, S. Garde, J. Phys. Chem. B **105**, 6380 (2001).

[27] N. Choudhury, J. Chem. Engg. Data **54**, 542 (2009).

[28] F. H. Stillinger, J. Solution Chem. **2**, 141 (1973).

[29] K. Lum, D. Chandler, J. D. Weeks, J. Phys. Chem. B **103**, 4570 (1999).

[30] J, Mittal, G. Hummer, Proc. Natl. Acad. Sci. U.S.A. **105**, 20103 (2008).

[31] D. Chandler, Nature, **437**, 640-647 (2005).

[32] T. M. Truskett, P. G. Debenedetti, S. Torquato, J. Chem. Phys. **114** 2401 (2001).

[33] A. Wallqvist, B. J. Berne, J. Phys. Chem. **99**, 2893 (1995).

[34] G. Hummer, J. C. Rasaiah, J. P. Noworyta, Nature **414**, 188 (2001).

[35] H. S. Ashbaugh, L. R. Pratt, M. E. Paulaitis, J. Clohecy, T. L. Beck, J. Am. Chem. Soc. **127**, 2808 (2005).

[36] N. Choudhury, B. M. Pettitt, J. Phys. Chem. **110**, 8459 (2006).

[37] N. Choudhury, J. Chem. Phys. **125**, 034502 (2005).

[38] N. Choudhury, J. Phys. Chem. C **111**, 2565 (2007).

[39] N. Choudhury, J. Phys. Chem. B **111**, 10474 (2007.

[40] T. Hotta, A. Kimura, M. Sasai, J. Phys. Chem. B. **109**, 18600 (2005).

[41] N. Choudhury, J. Chem. Phys. **132**, 064505 (2010).

[42] N. Choudhury, J. Chem. Phys. **133**, 154515 (2010).

[43] S. Jamadagni, T. M. Truskett, S. Garde, Proc. Natl. Acad. Sci. U.S.A. **102**, 9475 (2005).

[44] R. Zhou, X. Huang, C. J. Margulis, B. J. Berne, Science **305**, 1605 (2004).

[45] S. Sarupria, S. Garde, Phys. Rev. Lett. **103**, 037803 (2009).

[46] N. Giovambattsta, C. F. Lopez, P. J. Rossky, P. G. Debenedetti, Proc. Natl. Acad. Sci. U.S.A. **105**, 2274 (2008).

[47] N. Giovambattsta, P. G. Debenedetti, P. J. Rossky, Proc. Natl. Acad. Sci. U.S.A. **106**, 15181 (2009).

[48] Y. Levy, J. N. Onuchic, Annu. Rev. Biophys. Biomol. Struct. **35**, 389 (2006).

[49] H. K. Christenson, P. M. Claesson Science **239**, 390 (1988).

[50] H. K. Christenson, In *Modern Approaches to wettability: Theory and Applications, 1992*, M. E. Schrader, G. Loeb, Eds. Plenum: New York.

[51] Pashley, R. M.; McGuiggan, P. M.; Ninham B. W.; Evans, D. F. *Science* **1985**, *229*, 1088-1089.

[52] H. J. C. Jorgensen, J. D. Madura, C. J. Swenson, J. Am. Chem. Soc. **106**, 6638 (1984).

[53] H. J. C. Berendsen, J. R. Grigera, T. P. Straatsma, J. Phys. Chem. **91**, 6269 (1987).

[54] M. P. Allen and D. J. Tildesley, *Computer Simulation of Liquids*; Oxford University, New York, 1987.

[55] S. Garde, Private communication.

[56] M. V. Athawale, S. N. Jamadagni, S. Garde, J. Chem. Phys. **131**, 115102 (2009).

[57] P. -L. Chau, A. J. Hardwick, Mol. Phys. **93**, 511 (1998).

[58] J. R. Errington, P. G. Debenedetti, Nature **409**, 318 (2001).

[59] Z. Yan, S. V. Buldyrev, P. Kumar, N. Giovambattista, P. G. Debenedetti, H. E. Stanley, Phys. Rev. E **76**, 051201 (2007).

Figure Captions

Fig. 1: The normalized single particle density $g_{SO}(z)$ of water oxygen as a function of distance z from the model paraffin plate for different values of λ.

Fig. 2 (a) Solute-water potential of mean force $W_{SO}(z)$ of a water molecule as a function of diatance z from the model paraffin solute (plate) for values $\lambda = 0, 0.5$ and 1.
(b) Solvent induced PMF $\omega_{ind}(z)$ for values of $\lambda = 0, 0.25, 0.5, 0.75$, and 1.

Fig. 3: Orientational distribution functions of the (a) dipole moment vector $\mathrm{P}_{\mu}(\cos\ \theta)$ vs $\cos\theta$ (b) OH bond vector $\mathrm{P}_{OH}(\cos\ \psi)$ vs $\cos\psi$ and (c) $\mathrm{P}_{\perp}(\cos\ \phi)$ vs $\cos\phi$ of the water molecules for different values of λ.

Fig. 4: Histograms of water molecules with n hydrogen bonds f_n^{HB} for water in plate-water systems with $\lambda = 0, 0.25, 0.5, 0.75, 1$ and bulk.

Fig. 5: Average number of hydrogen bonds ($< n_{HB} >$) per water molecules as a function of perpendicular distance z from the solute plate for different paraffin-like plates (with different values of λ).

Fig. 6: Local compressibility $\chi_T(z)$ of a slab of water of width 1 Å at different locations along the perpendicular direction of the plate for different values of λ.

Fig. 7: Normalized fluctuation $K_N(z)$ of a slab of water of width 1 Å at different locations along the perpendicular direction of the plate for different values of λ and for bulk water.

Fig. 8: Water-water correlations at different interfaces with different λ values as calculated through intermolecular water (a) oxygen-oxygen pair correlation function $g_{OO}(r)$ and (b) oxygen-hydrogen pair correlation function $g_{OH}(r)$ near the paraffin plate measured in a 1 Å thick slab placed parallel to the interface located at the half density plane of water.

Fig. 9: (a) First shell tetrahedral order parameter, q_4 and (b) second shell orientational order parameter Q_6 for water at different slabs parallel to the surfaces as a function of distance from the plate for different plates of varying λ values.

Fig. 10: Normalized one-particle density profile, $\rho(z)/\rho_0$ as a function of perpendicular distance from the plate, z (a) for $\lambda = 1.0$ and (b) for $\lambda = 0.75$ plate-water systems. The red lines in (b) is for plates with interplate distance, $r_0 = 12$ Å and the black line is for the same with $r_0 = 10$ Å.

Fig. 11: Normalized one-particle density profile, $\rho(z)/\rho_0$ as a function of perpendicular distance from the plate, z for (a) $\lambda = 0.5$ and for (b) $\lambda = 0.75$ plate-water systems. The red lines in (b) is for plates with interplate distance, $r_0 = 14$ Å and the black line is for the same with $r_0 = 12$ Å.

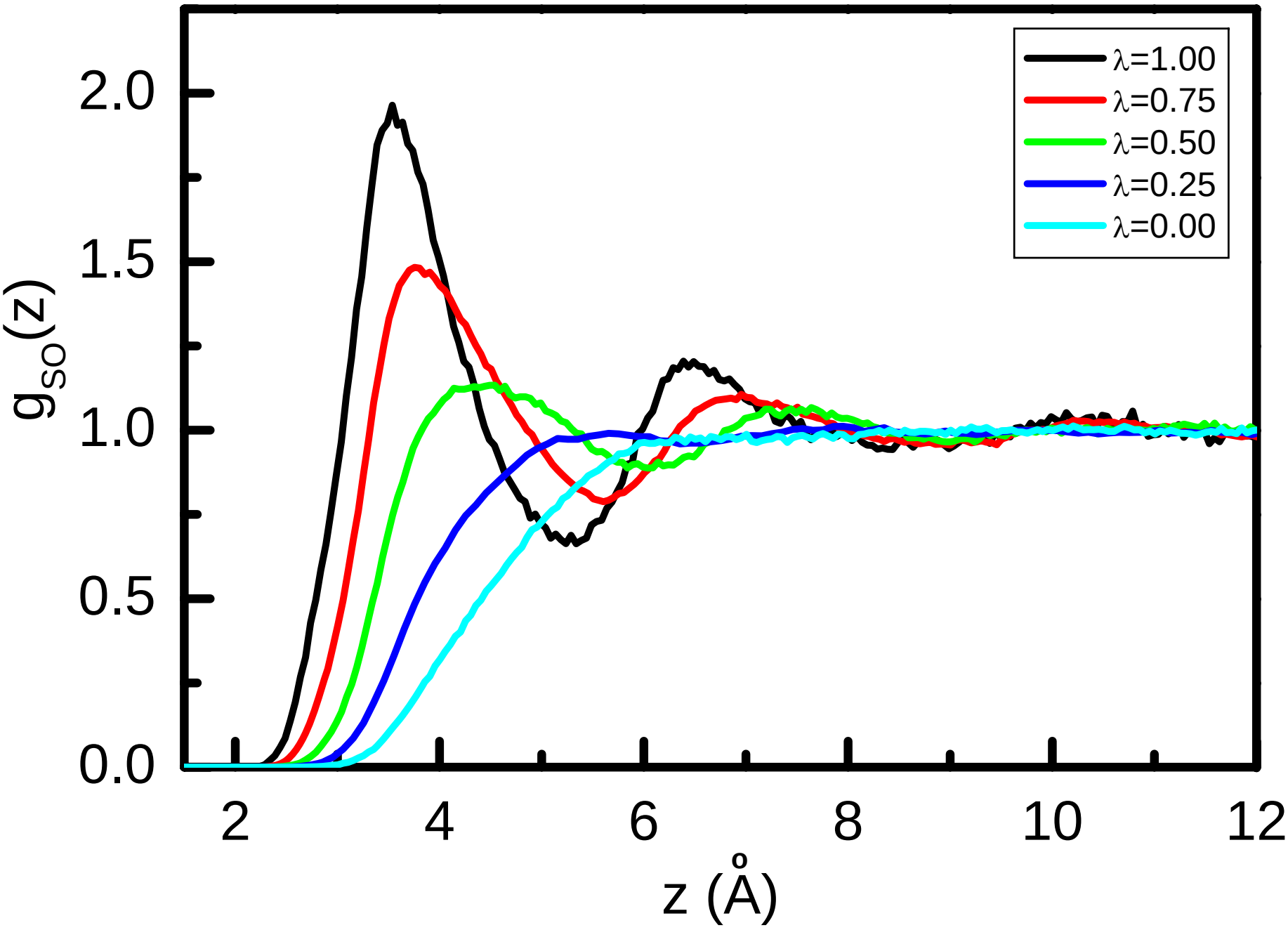

Fig. 1

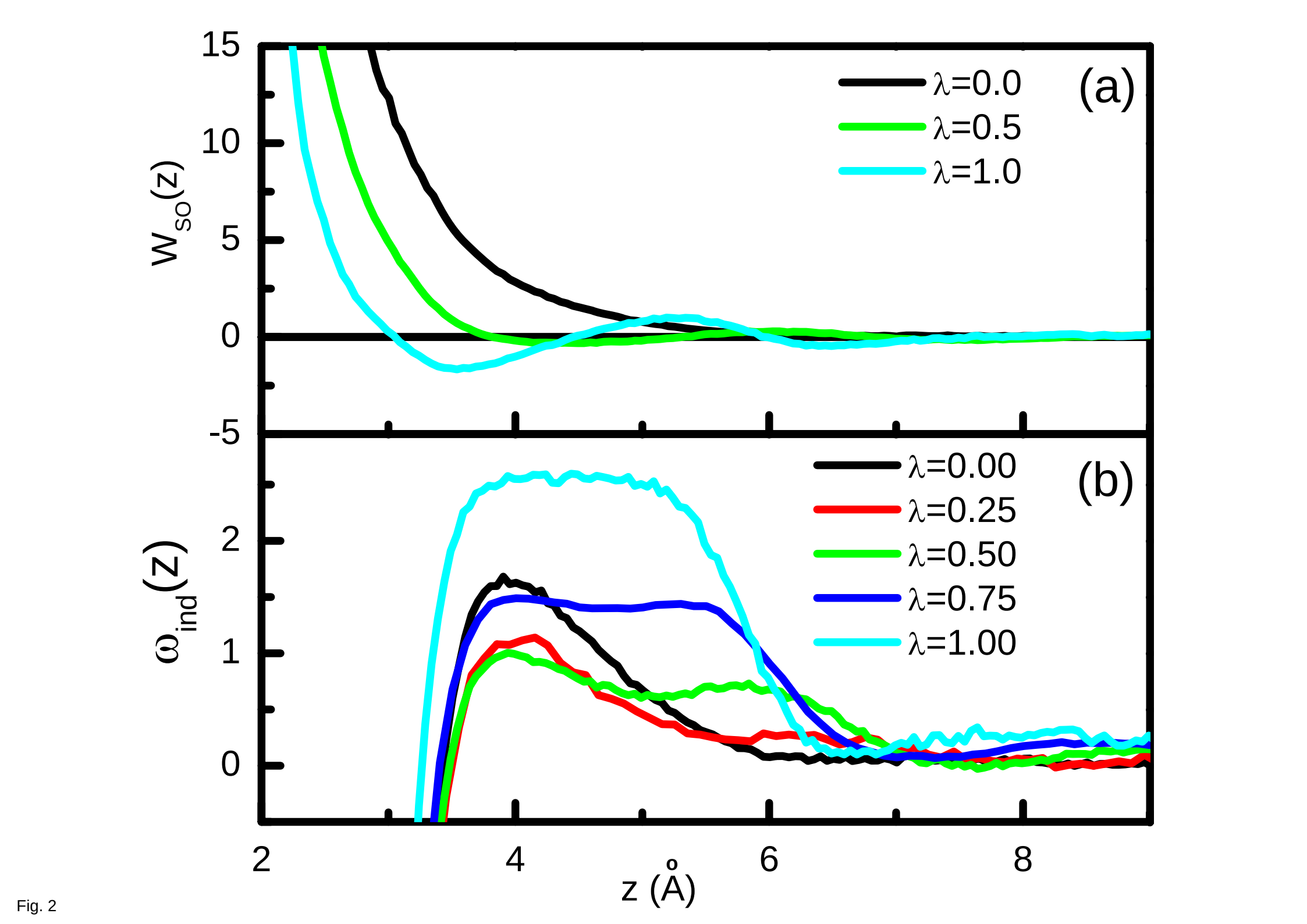
15
10
5
0
-5
$W_{SO}(z)$
λ=0.0
λ=0.5
λ=1.0
(a)
2
1
0
$\omega_{ind}(z)$
λ=0.00
λ=0.25
λ=0.50
λ=0.75
λ=1.00
(b)
2
4
6
8
z (Å)

Fig. 2

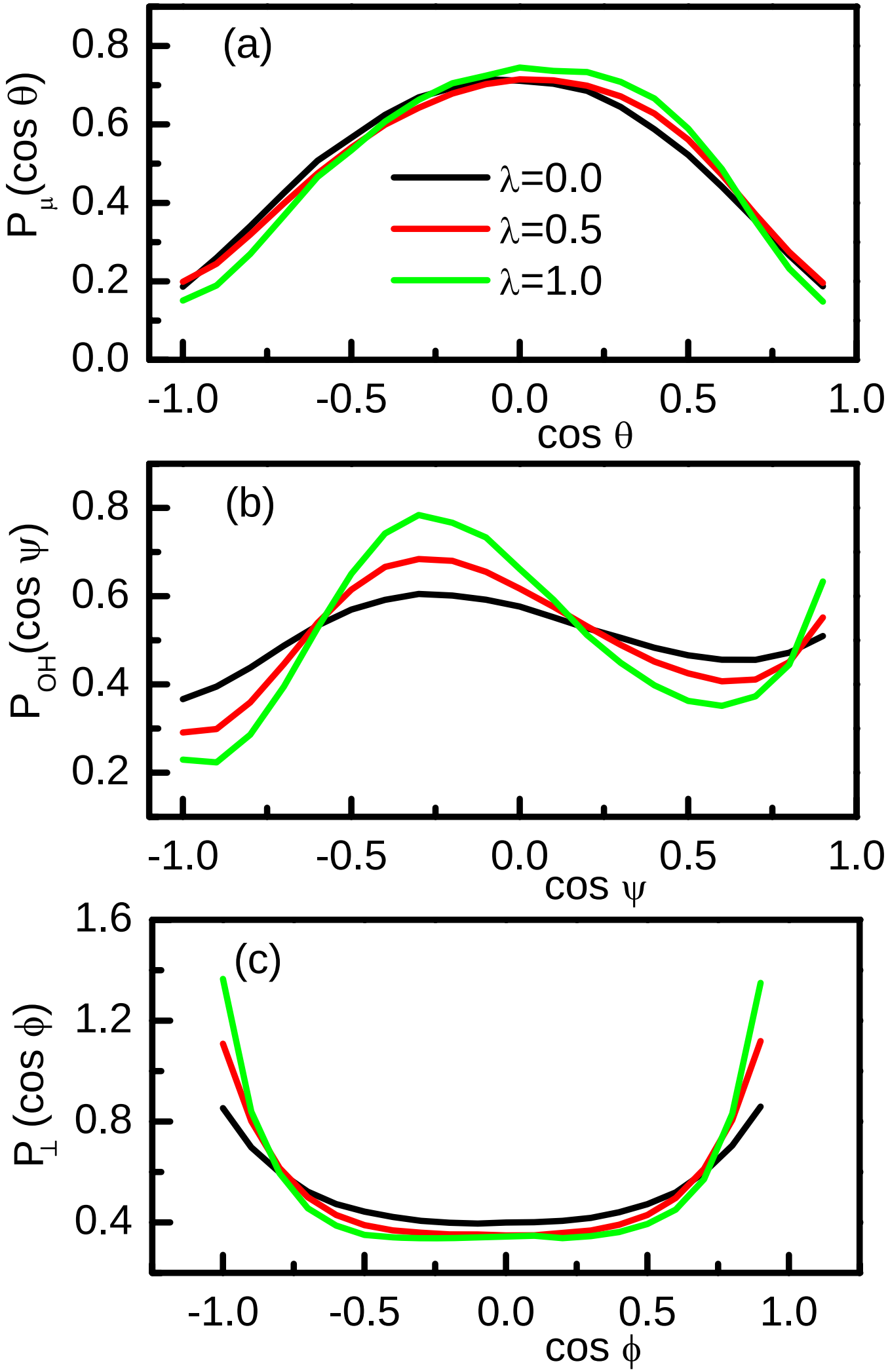
(a)
0.8
0.6
0.4
0.2
0.0
$P_\mu(\cos\theta)$
λ=0.0
λ=0.5
λ=1.0
-1.0
-0.5
0.0
0.5
1.0
cos θ
(b)
0.8
0.6
0.4
0.2
$P_{OH}(\cos\psi)$
-1.0
-0.5
0.0
0.5
1.0
cos ψ
(c)
1.6
1.2
0.8
0.4
$P_\perp(\cos\phi)$
-1.0
-0.5
0.0
0.5
1.0
cos ϕ

Fig. 3

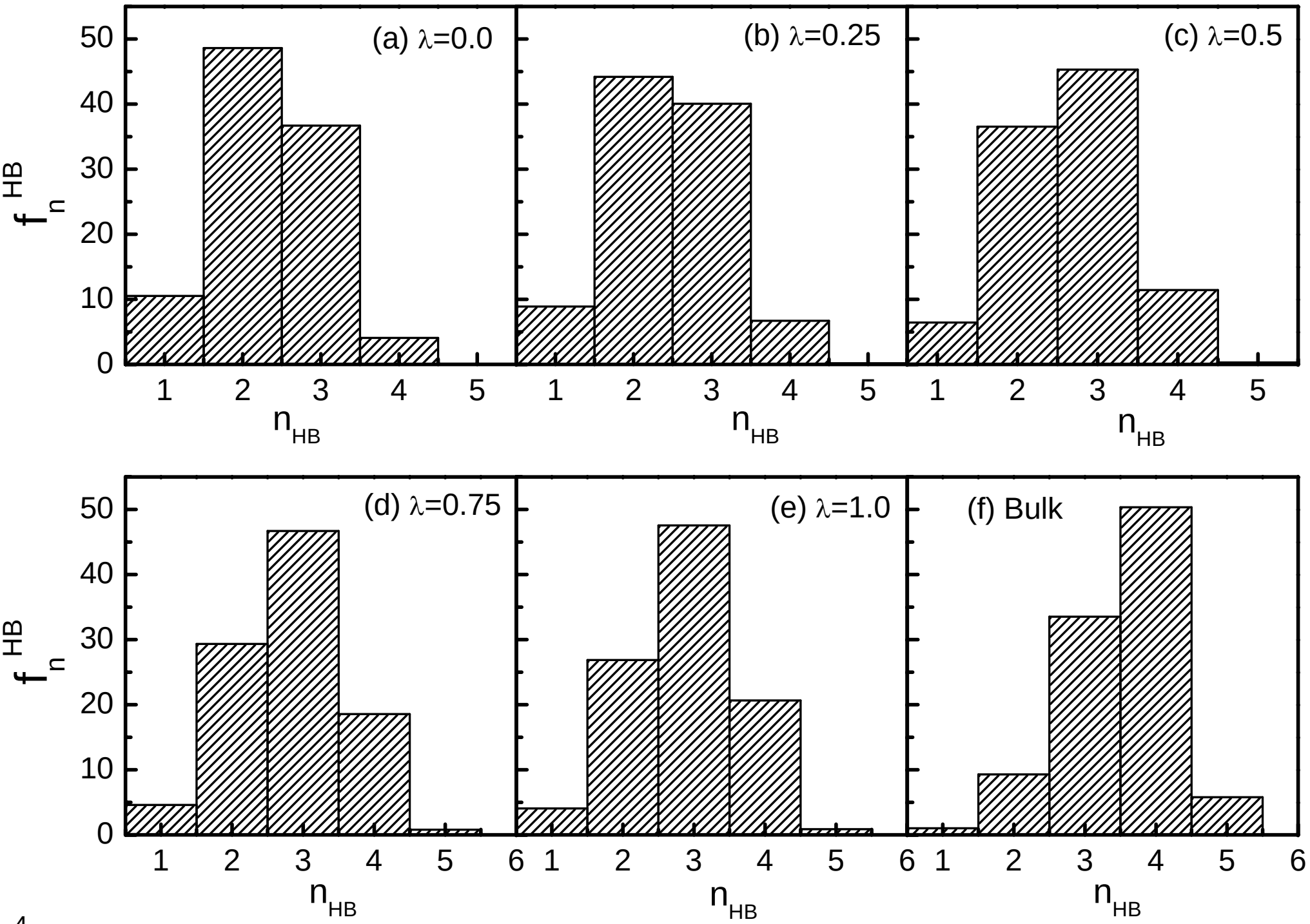
(a) λ=0.0
(b) λ=0.25
(c) λ=0.5
(d) λ=0.75
(e) λ=1.0
(f) Bulk
f_n^{HB}
n_{HB}
0
10
20
30
40
50
1
2
3
4
5
6

Fig. 4

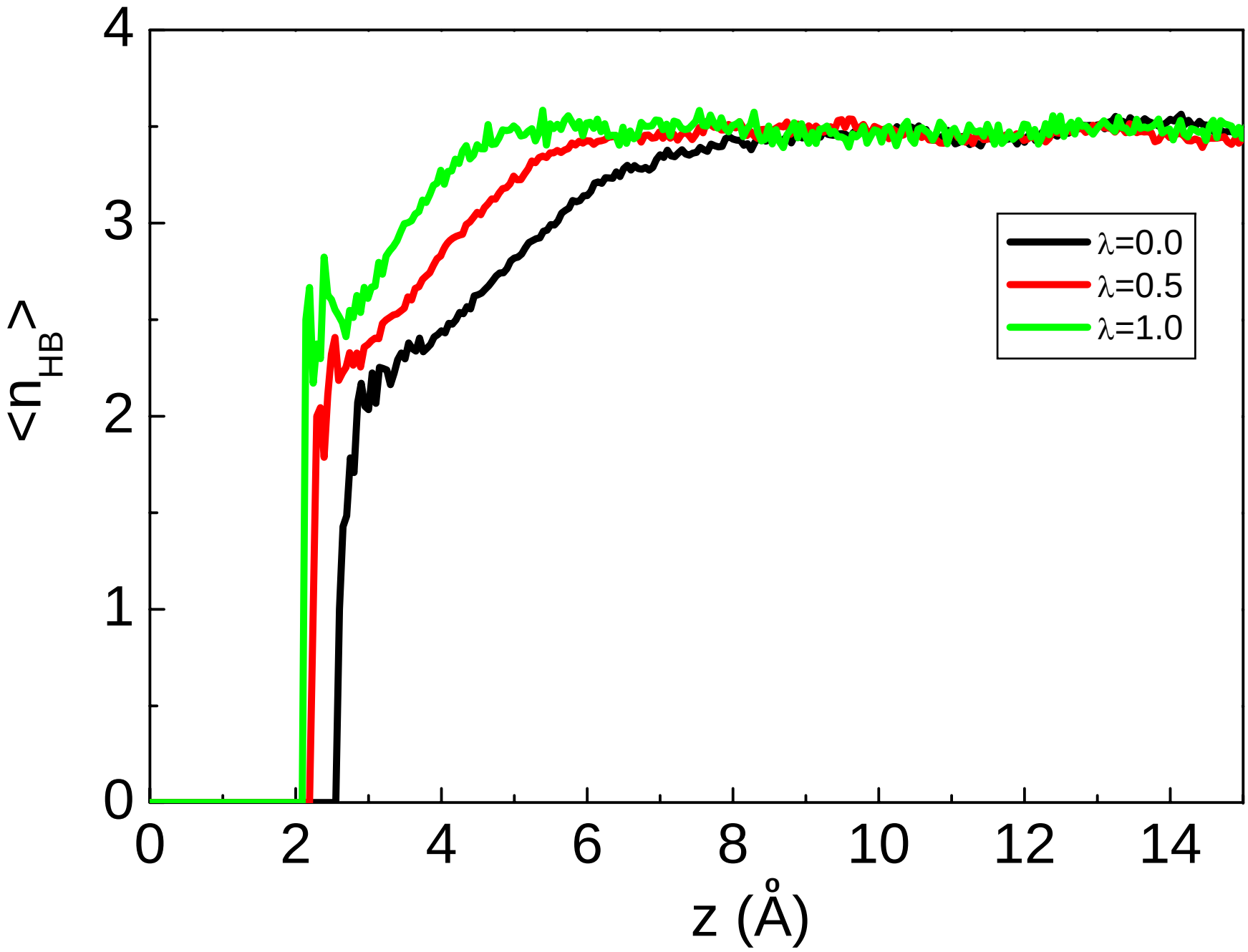

Fig.5

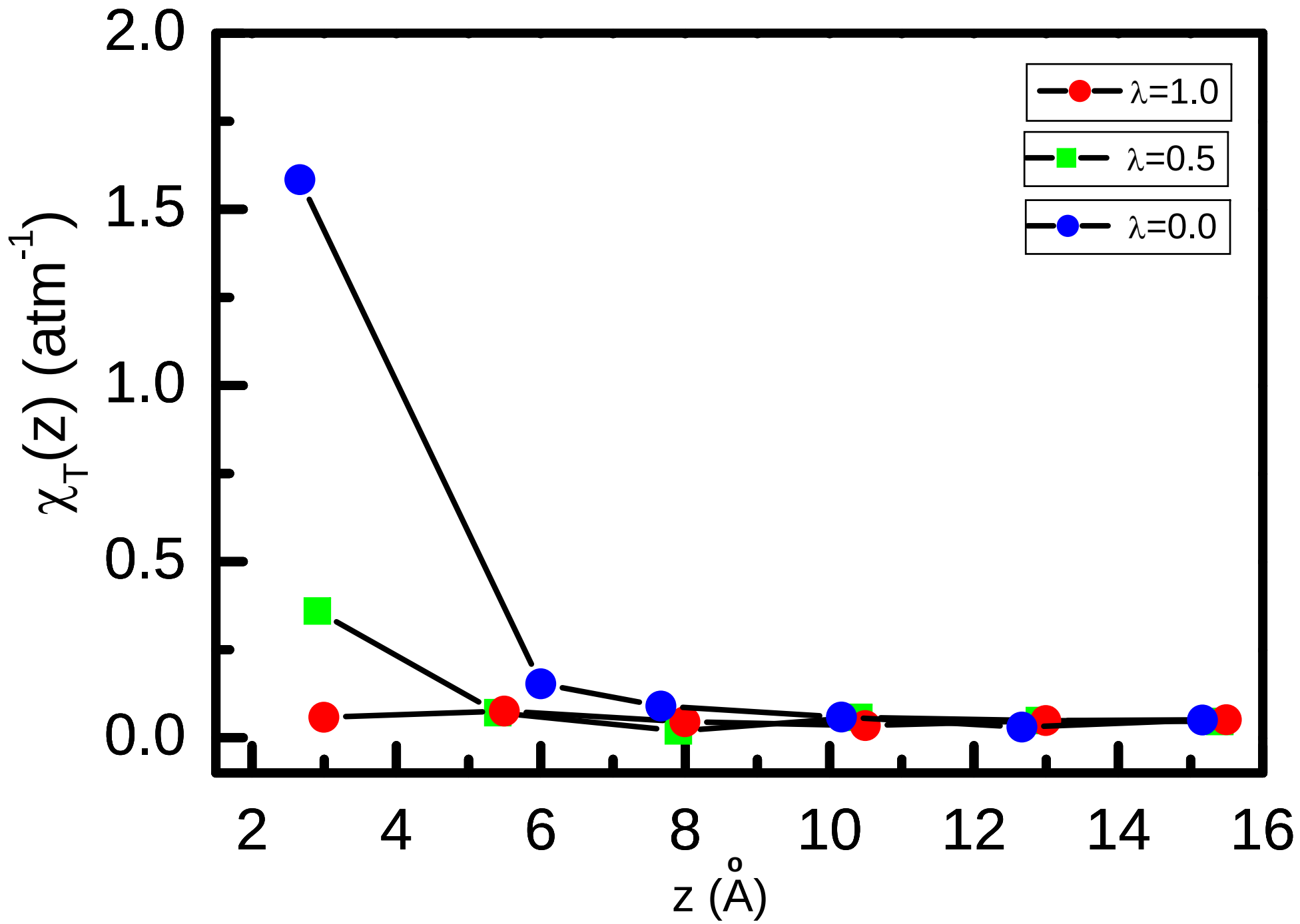

Fig. 6

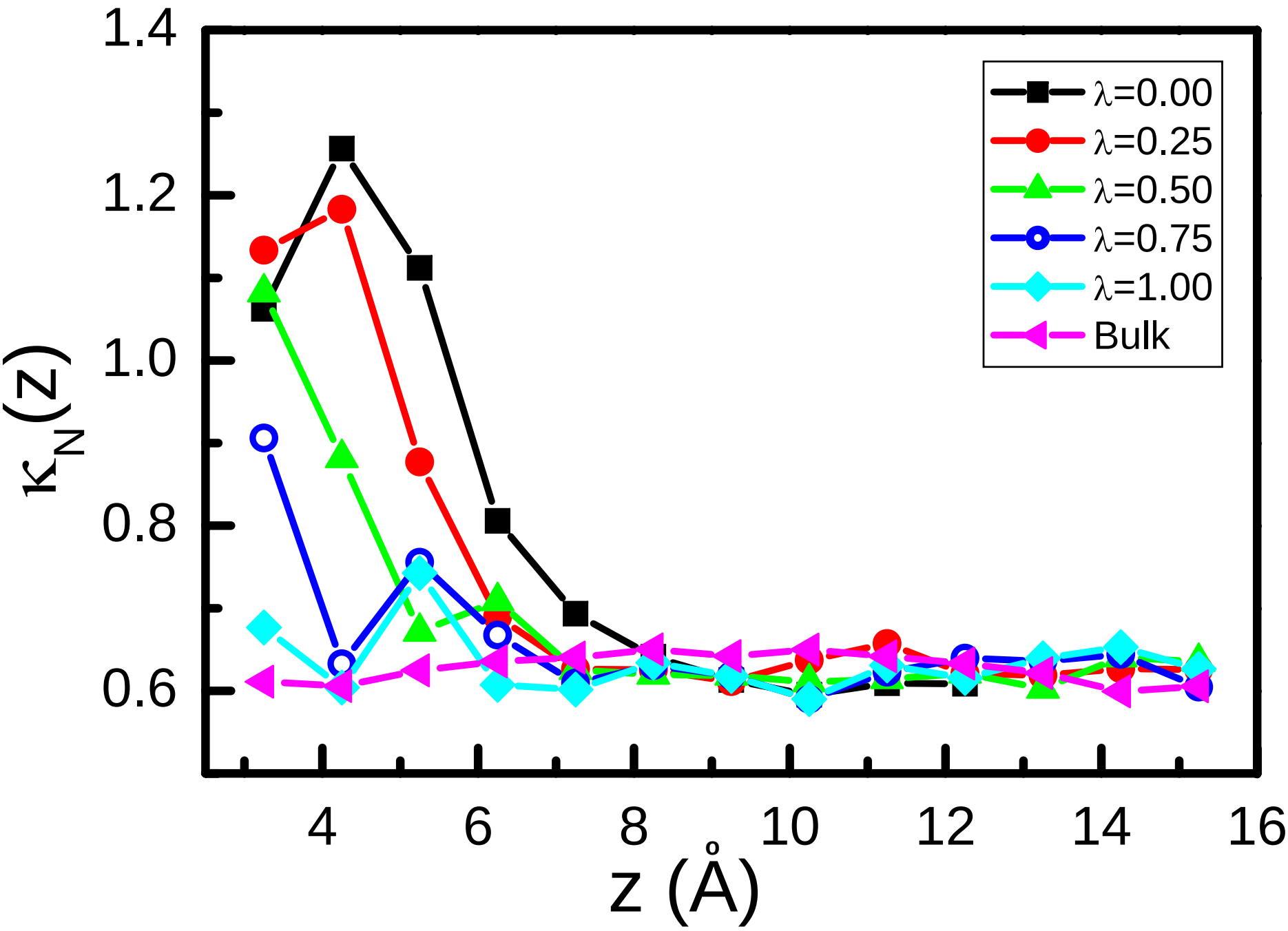
1.4
1.2
1.0
0.8
0.6
$\kappa_N(z)$
4
6
8
10
12
14
16
z (Å)
λ=0.00
λ=0.25
λ=0.50
λ=0.75
λ=1.00
Bulk

Fig. 7

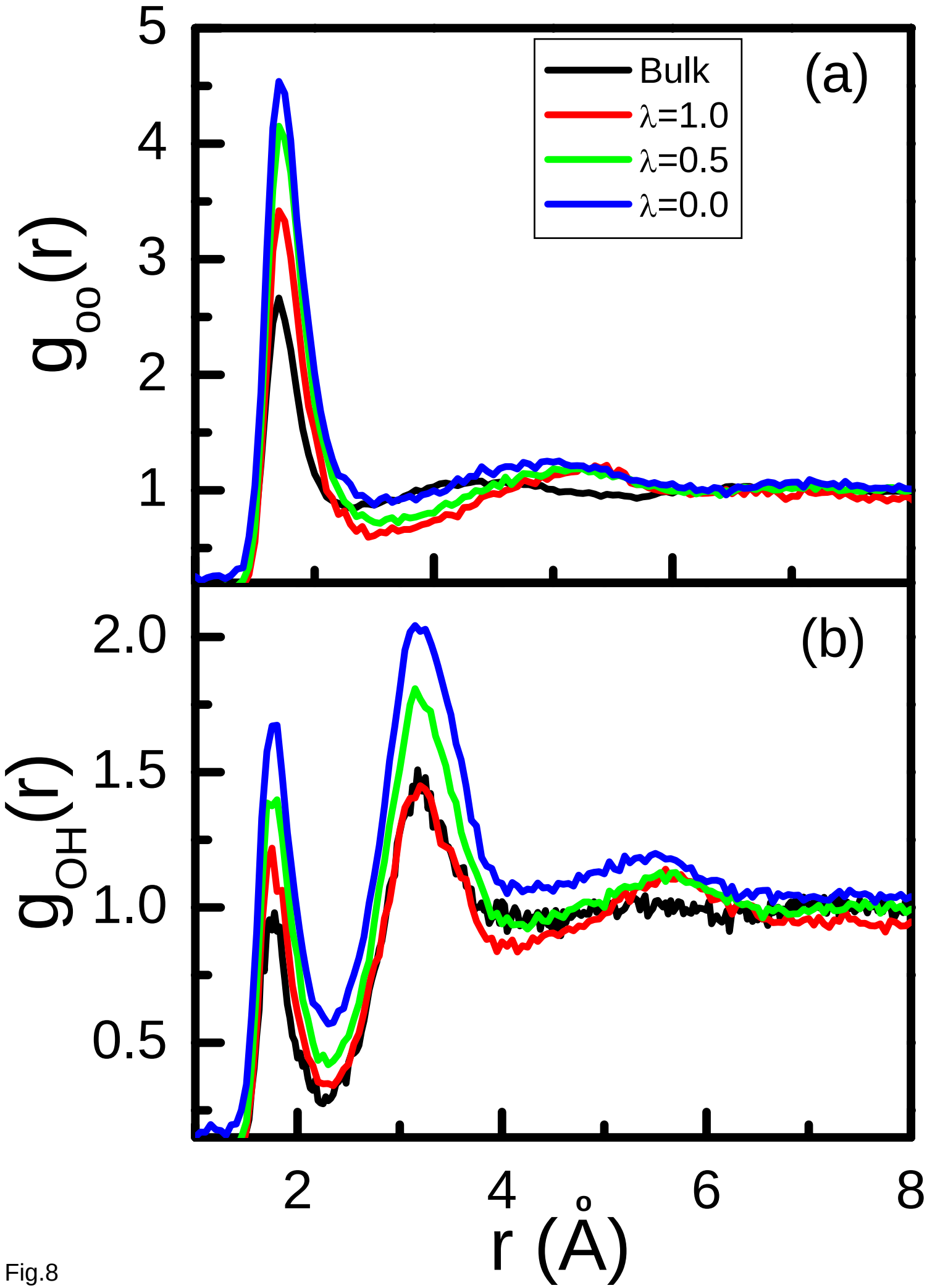

Fig.8

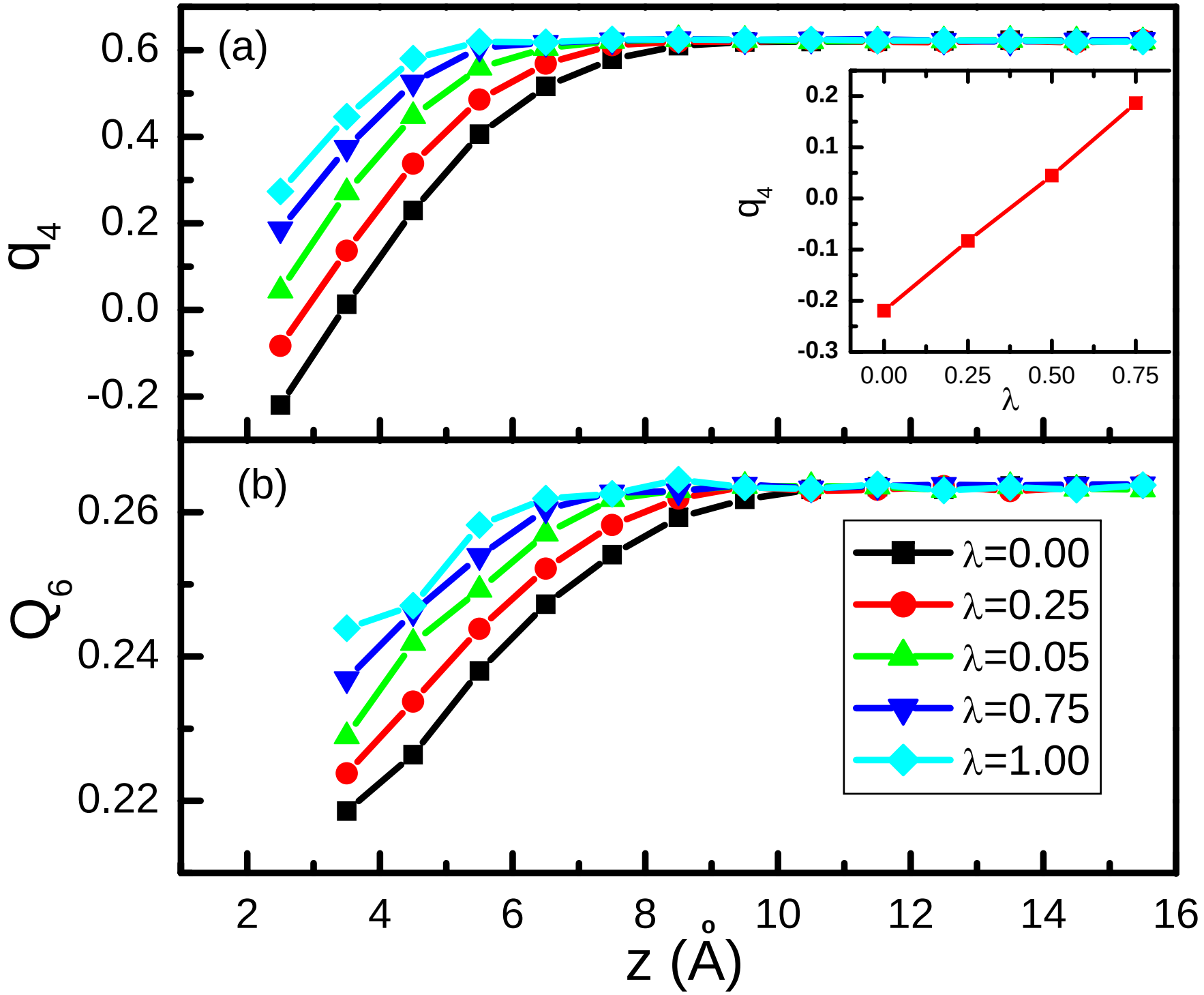
(a)
(b)
q_4
Q_6
z (Å)
λ=0.00
λ=0.25
λ=0.05
λ=0.75
λ=1.00
0.6
0.4
0.2
0.0
-0.2
0.26
0.24
0.22
2
4
6
8
10
12
14
16
0.2
0.1
0.0
-0.1
-0.2
-0.3
0.00
0.25
0.50
0.75
λ

Fig. 9

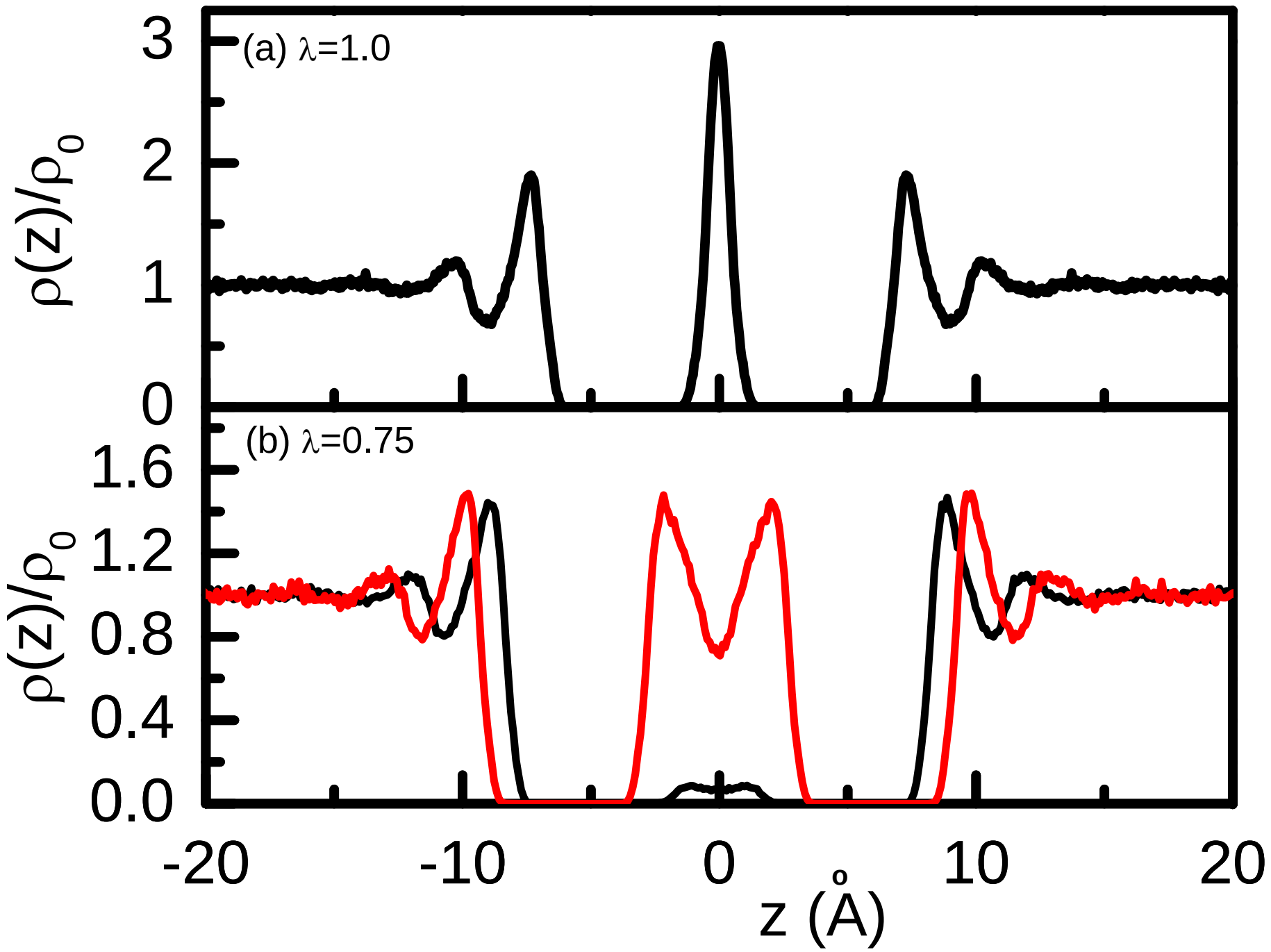

Fig. 10

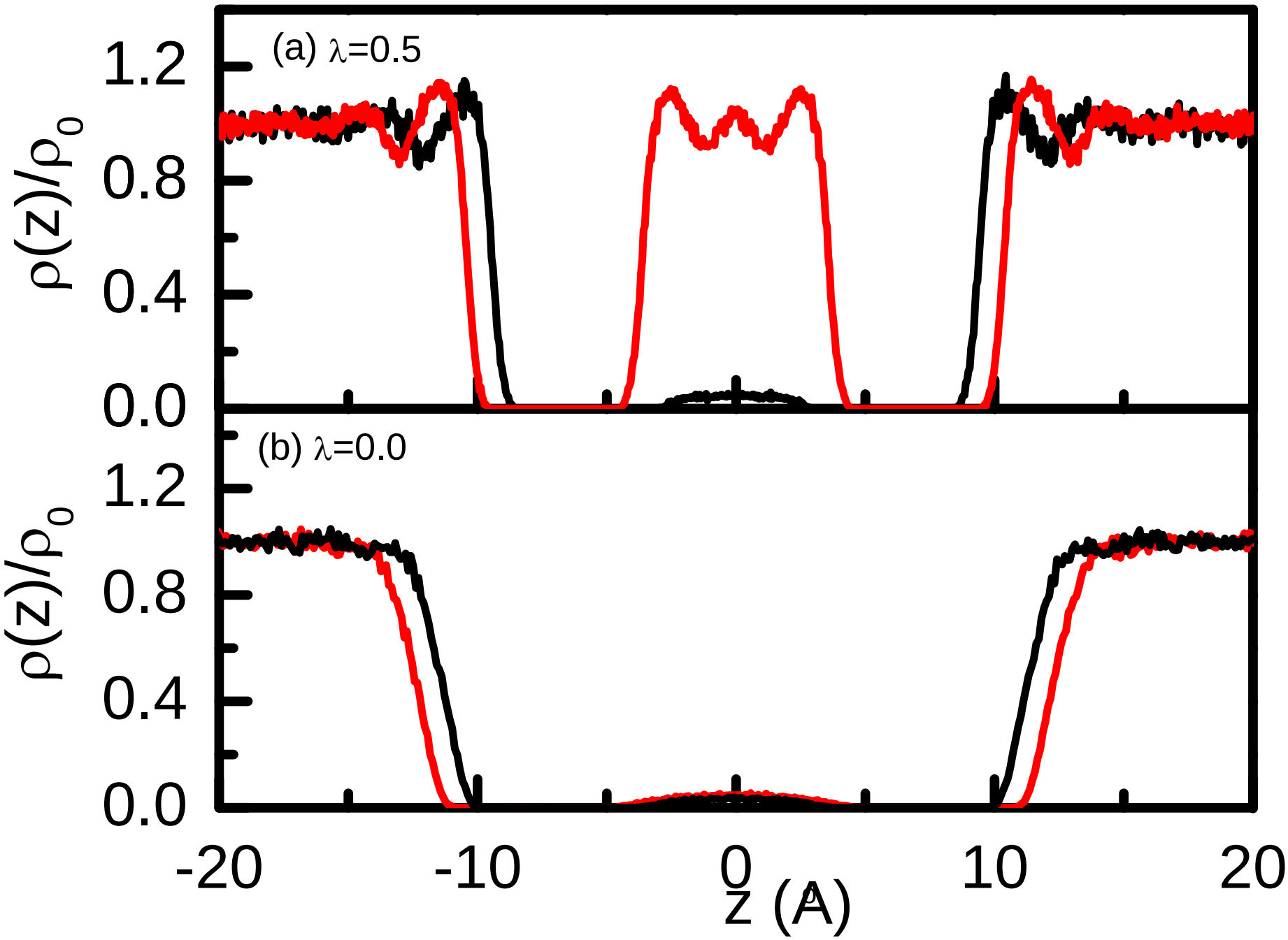

Fig. 11